

Article

Unprecedented Rainfall and Moisture Patterns during El Niño 2016 in the Eastern Pacific and Tropical Andes: Northern Perú and Ecuador

Janeet Sanabria ^{1,*}, Carlos M. Carrillo ²  and David Labat ¹

¹ UMR 5563 GET, Université de Toulouse–CNRS–IRD–OMP–CNES, CEDEX 9, 31062 Toulouse, France; david.labat@get.omp.eu

² Department of Earth and Atmospheric Sciences, Cornell University, Ithaca, NY 14853, USA; mcarrillo_cruz@hotmail.com

* Correspondence: janeetsanabria@hotmail.com

Received: 3 November 2019; Accepted: 26 November 2019; Published: 3 December 2019



Abstract: Using vertically integrated water vapor and its convergence, associated with large-scale and regional atmospheric circulation, we found two patterns of rainfall over the Eastern Pacific (EP) and the tropical Andes—with a focus in Ecuador and northern Perú—during three recent El Niño events: 1983, 1998, and 2016. Although these three events were the strongest El Niños, the different sources of moisture contribute to different rainfall patterns between El Niño 1983–1998 and 2016. In the region, the spatial pattern of precipitation during El Niño 2016 presents an unprecedented out-of-phase atmospheric response consistent and verified with water vapor transport when compared with El Niño 1983–1998. During El Niño 2016, precipitation in the Andes was enhanced by moist air transported from the Amazon—with an opposite regime compared to the subsidence that dominated in 1983–1998. During the 1983–1998 El Niño, the source of moisture to feed the EP was enhanced by upper-level divergence (300 hPa), which supports moisture influx by middle levels in the EP. In El Niño 2016, this divergent upper-level flow migrated north, followed by the companion moisture. This study illustrates a link between upper-level large-scale circulation and low-level regional mechanisms on the moisture transport in determining different rainfall patterns during El Niño events.

Keywords: moisture transport; moisture convergence; extreme rainfall; strong El Niño events; Eastern Pacific; tropical Andes

1. Introduction

El Niño corresponds to a global scale climate pattern that is commonly observed in sea surface temperature (SST) anomalies in the Central Pacific Ocean [1–6]. It drives well-known temporal and spatial patterns of rainfall in the Central Pacific (CP) and Eastern Pacific (EP) [2,7,8], as shown in Figure 1. The rainfall anomaly in the EP is highly associated with SST anomalies in remote (El Niño 3.4) and local (El Niño1 + 2) regions [9–13]. Transport of atmospheric moisture responds to the El Niño seasonal progression, which moves eastward along the warm equatorial SST. In the Andes, along the vicinity of northern Perú and Ecuador, the variability of rainfall (dry and wet) during El Niño years is not only related to remote moisture from the Pacific Ocean but also by moist air from the Amazon basin [14–16]. This claim has been controversial for years [16,17] (atmospheric subsidence in the Amazon basin constitutes a common pattern during El Niño years [18]). Thus, the transport of water vapor from the ocean and local topography of the Andes could lead rainfall production toward the continent [19,20] when land-sea breeze intersects the coastal area [9,11]. Evidence of this source of moisture from the Amazon has been limitedly explored [21], so this study investigates whether this moist transport could have occurred during El Niño 2016.

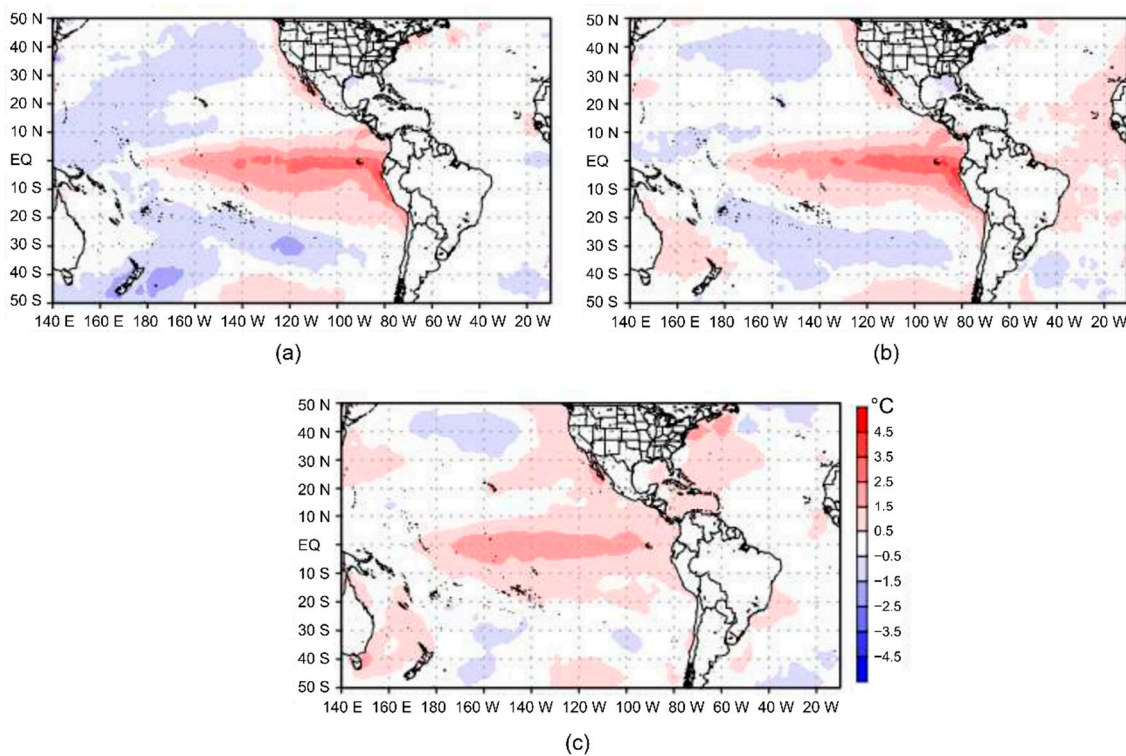


Figure 1. January through April (JFMA) composites of sea surface temperature anomalies ($^{\circ}\text{C}$) over the Tropical Pacific during the three strong El Niño events (a) 1982/1983, (b) 1997/1998 and (c) 2015/2016. These anomalies are obtained from the HadISST data set over the period 1950–2016.

El Niño can be characterized by two regimes: East Pacific and Central Pacific ENSO [22–24], as characterized by significant SST anomalies. During El Niño 1983 and 1998 (hereafter 1983–1998), the EP exhibited positive precipitation anomalies with negative sea level pressure (SLP) anomalies and northerly winds, consistent with the southward migration of the Intertropical Convergence Zone (ITCZ) [10,25–27]. However, this atmospheric configuration was not the case during El Niño 2016, which showed opposite conditions: negative precipitation anomalies with high SLP and the ITCZ located northward of its climatology position during El Niño years [6,28–32]. During the 2016 El Niño event, the different pattern of configuration motivates us to investigate whether this case can be robust enough to show this out-of-phase pattern. Specifically, to question what the role of the regional aspects of atmospheric conditions is in the two responses of rainfall under similar El Niño events.

The focus of the present study is how similar global El Niños (1983–1998 and 2016) can contribute to different patterns of rainfall over the EP and the tropical Andes of Ecuador and Perú. Why the pattern of rainfall has a different response to El Niño, and whether these differences are on local variability is investigated (e.g., Niño 1 + 2; Figure 2). Fundamentally, could the Andes at the Equator have different responses with similar global El Niños, as defined by El Niño 3.4 SST? We hypothesize that rainfall anomaly in the EP can experience out-of-phase patterns in similar El Niño events as measured by the large-scale (El Niño 3.4). As these patterns must agree with the balance of water and atmospheric radiation, the precipitation in the Andes could change according to local factors as a key ingredient for the out-of-phase pattern. The hypothesis is tested by analyzing variations in moisture transport, rainfall, and atmospheric circulation changes.

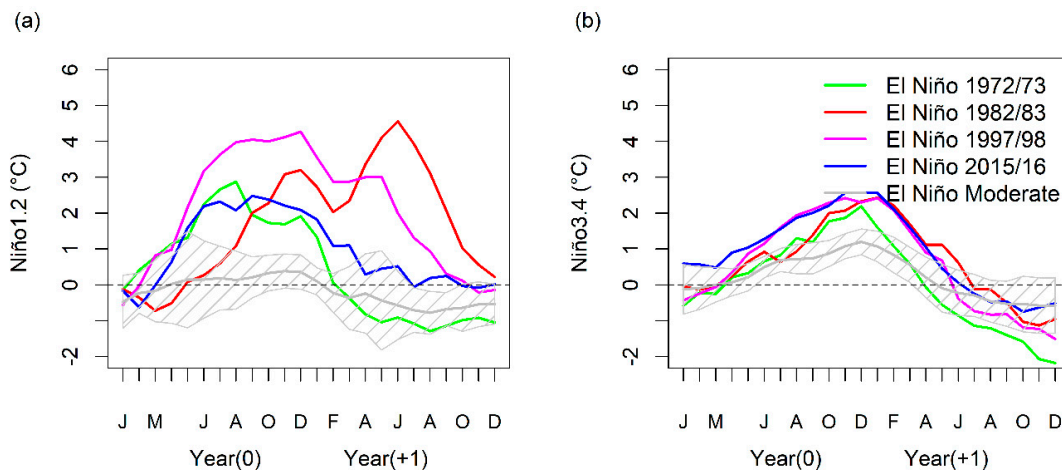


Figure 2. Evolution of the sea surface temperature anomalies in the (a) Niño 1.2 and (b) Niño 3.4 region during the four strong El Niño events (1972/1973, 1982/1983, 1997/1998, and 2015/2016) and the composite of moderate events. The Niño 1.2 and Niño 3.4 region from the HadISST data set over the period 1950–2016. The composite for moderate events includes 12 events from 1950 to 2016 (i.e., years 1957/1958, 1963/1964, 1965/1966, 1968/1969, 1969/1970, 1977/1978, 1987/1988, 1991/1992, 1994/1995, 2002/2003, 2004/2005, and 2009/2010). The hatching in the grey line represents the dispersion (standard deviation) among the 12 moderate El Niño events.

2. Data and Methodology

Using the vertically integrated water balance equation, we consider that the spatial pattern of rainfall and atmospheric water vapor are comparable [33].

2.1. Precipitation

The analysis is based on monthly observed precipitation and reanalysis, which covers the period 1979–2016 at a spatial resolution of $0.5^\circ \times 0.5^\circ$. Observational and reanalysis datasets were re-gridded to a common grid. We used 145 meteorological stations obtained from the Peruvian National Weather Service (SENAMHI), accessed from this site <https://www.senamhi.gob.pe/?p=estaciones>. Quality control was performed using a regional vector method [12,34], which considers elevation, watershed boundaries, and latitude. Anomalies were computed using a climatology of 37 years (1979–2016).

2.2. Moisture Transport

We used the European Centre for Medium-Range Weather Forecasts (ECMWF) interim Reanalysis (ERA-interim) [35,36] to compute moisture transport and to verify atmospheric circulation changes during the selected El Niño events. ERA-interim covers the period from 1979 to the present and has 37 pressure levels from 1000 to 1 hPa with a horizontal resolution of $0.5^\circ \times 0.5^\circ$ (about 50 km). ERA-interim was obtained from <http://apps.ecmwf.int/datasets/data/interim-full-modala/levtype=sfc/>. ERA-interim over South America has shown low error in precipitation [37,38], and it has a reliable representation of the moisture source over the tropics [39,40]. The hydrological cycle of ERA-interim shows an improved forecasting skill compared to previous ERA-reanalysis [41].

To investigate the link of atmospheric moisture flux on the rainfall, we used the integrated water vapor transport:

$$\vec{Q} = Q_u i + Q_v j, \tag{1}$$

and computed its convergence $(-\nabla \cdot \vec{Q})$ from ERA-interim. The zonal (Q_u) and meridional (Q_v) water vapor transport are computed over the atmospheric column (from the surface to 100 hPa). The \vec{Q} is defined with $Q_u = \frac{1}{g} \int_{surface}^{100-hPa} q u dp$ and $Q_v = \frac{1}{g} \int_{surface}^{100-hPa} q v dp$. Here, q defines specific humidity, g is

the gravity constant, and u and v the zonal and meridional wind. The water vapor and precipitation are linked with the atmospheric water balance equation:

$$\frac{\partial w}{\partial t} + \nabla \cdot \vec{Q} = E - P, \quad (2)$$

which describes the atmospheric hydrological balance expressed as \vec{Q} convergence ($-\nabla \cdot \vec{Q}$), which is balanced by the difference between precipitation (P) and evaporation (E); w is the precipitable water (total column water vapor), and its change is assumed to be negligible over a relatively long period (e.g., [41,42]).

2.3. EOF/PC Analysis on C and E Indices

The dominant pattern of moisture and precipitation, associated with SST in the EP and CP, were obtained using both an empirical orthogonal function (EOF) and regression analysis [43]. The technique constructs a regression model based on the statistical dominant principal components (PCs) as its predictors—in order to find the regression coefficients between the predictand and the independent PCs of the predictor fields. Thus, the technique separates the moisture pattern associated with dominant statistical eigenvectors: two types of ENSO (E and C). In our study, the PCs regression construct the predictand for precipitation and $-\nabla \cdot \vec{Q}$ anomalies, using the predictors of the E and C indices. These indices (E index and C index) were constructed with an EOF analysis on sea surface temperature (EOF; with EOF1 [SST] and EOF2 [SST]) as defined in [23]:

$$\text{E index} = (\text{PC1} - \text{PC2}) / \sqrt{2}, \quad (3)$$

and

$$\text{C index} = (\text{PC1} + \text{PC2}) / \sqrt{2}. \quad (4)$$

Rainfall during El Niño events (1983, 1998, and 2016) is portrayed in relation to \vec{Q} convergence ($-\nabla \cdot \vec{Q}$), specific humidity (q), vertical motion (ω), and winds. Variability of \vec{Q} convergence allows examining the changes in the atmospheric balance of the hydrological cycle. \vec{Q} reflects the general circulation in the lower atmosphere [44]. The specific humidity is related to moisture transport (\vec{Q}) and its variability [45] by its definition $\vec{Q} = \frac{1}{g} \left[\int_{\text{surface}}^{100-hPa} q \vec{u} dp + \int_{\text{surface}}^{100-hPa} q \vec{v} dp \right]$. Increases in moisture transport (\vec{Q}) and q are associated with extreme rainfall events [46]. The vertical structure of q identifies the dry and wet atmosphere associated with anomalous global and continental-scale circulation (convection, subsidence, and low-and-high level circulation). This vertical structure was constructed for the tropical region (between 2° S and 7.5° S). The analysis was done for the seasonal anomaly composites (the JFMA rainy period). The comparison of observed and estimated precipitation ($-\nabla \cdot \vec{Q}$) is helpful for the reliability of moisture transport variability.

3. Results

3.1. The EOF Modes of \vec{Q} , its Convergence ($-\nabla \cdot \vec{Q}$), and Rainfall Variability

EOF and regression analysis applied on precipitation and vertically integrated water vapor transport (\vec{Q}) are shown in phase-space plots (Figures 3a and 4a) and spatial patterns (Figures 3b and 4b). They reveal the Central Pacific (C) and East Pacific (E) indices of El Niño types. The precipitation index features for El Niño 1983 and 1998 are projected onto the E pattern ($P \approx 0$) with significant positive values, while the El Niño 2016 event has E values near to zero ($C \approx -2.2$). The $-\nabla \cdot \vec{Q}$ follows similar behavior but with negative values due to a negative sign of $\nabla \cdot \vec{Q}$. In Figures 3b and 4b, the EOF

patterns show different anomalies with center in the EP and CP. The EP and CP rainfall patterns agree with the water vapor transport and its convergence sources. The EP precipitation pattern expands over the Eastern Pacific near the edge of Ecuador and northern Perú, with northwesterly \vec{Q} anomalies flux and positive rainfall anomalies consistent with other studies [33,47]. In the CP pattern, precipitation is confined to the west Pacific (around 5° N) associated with weak $-\nabla \cdot \vec{Q}$ and southeasterly \vec{Q} anomaly fluxes (Figure 4b). For both CP and EP patterns, the Amazonian region is a dry anomaly (negative precipitation anomalies), which is the common understanding, and the signal is stronger for the EP. These results indicate that moisture transport propagates from the Central Pacific that reaches the EP, but they present a different magnitude and shifting location, which impacts rainfall along the EP.

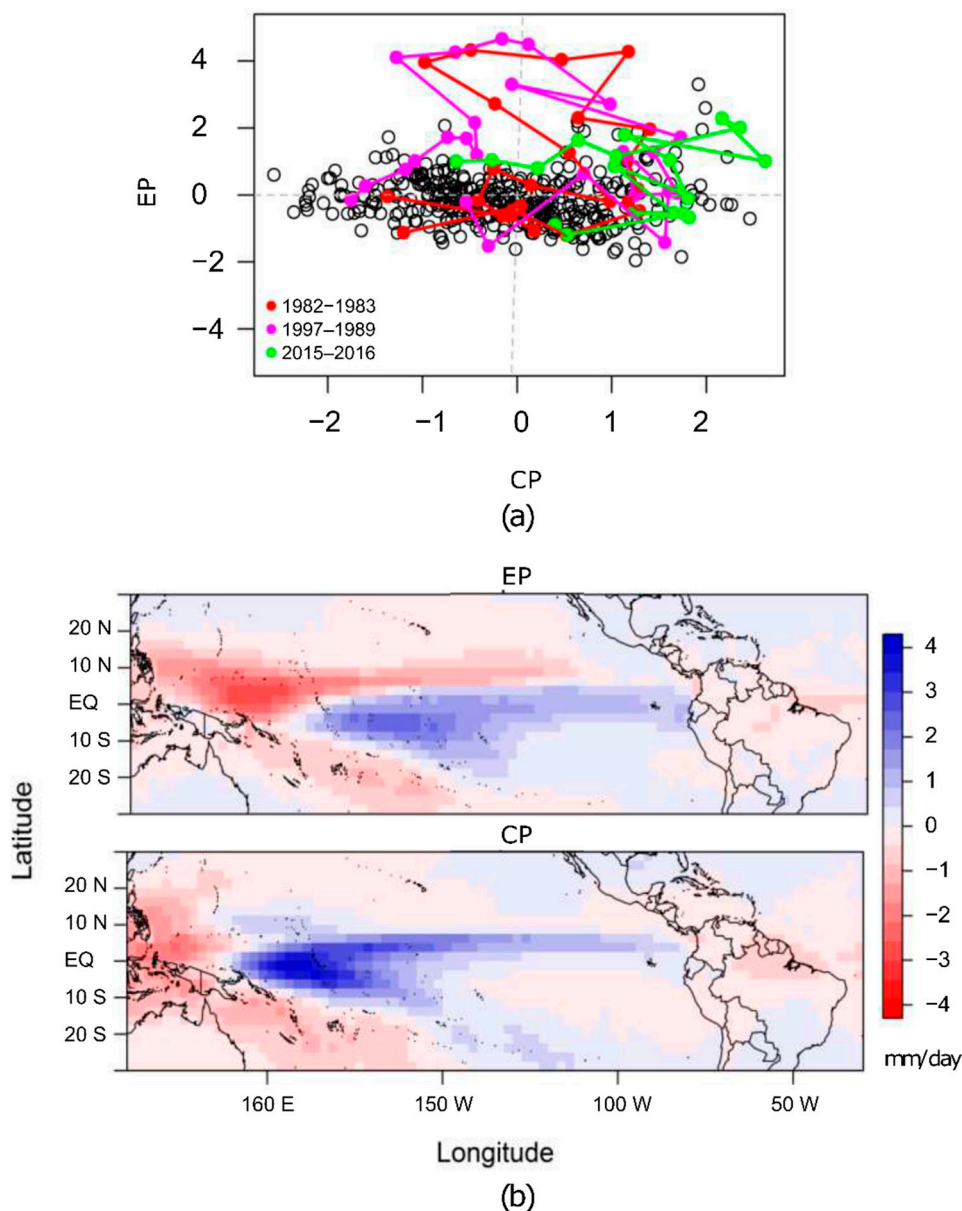


Figure 3. (a) Phase space of the evolution of the first dominant pattern of precipitation obtained using rotated Empirical Orthogonal Function (EOF). Their evolutions for three El Niño events (1983, 1998, and 2016) are highlighted with lines connecting the dots for the months between January of the first El Niño year and December of the second year. (b) Patterns of rainfall anomalies (EP and CP) associated with E and C indices. Indices are defined as in Ref. [23] from the HadISST data set over the period 1964–2016. Precipitation data were used from ERA-Interim reanalysis for the period 1979–2016.

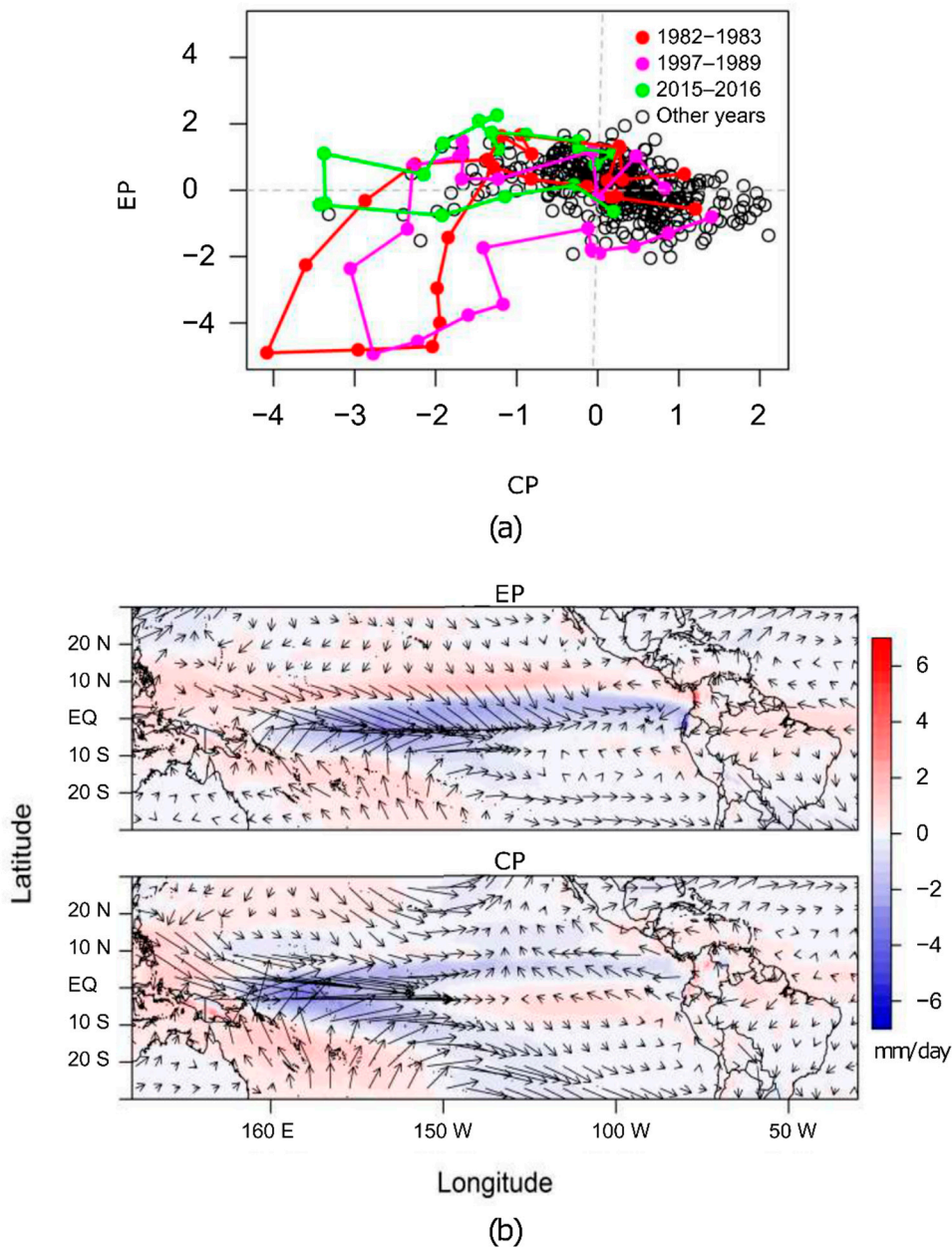


Figure 4. (a) Phase space of the evolution of the first dominant pattern of vertically integrated water vapor transport convergence ($-\nabla \cdot \vec{Q}$) obtained using rotated Empirical Orthogonal Function (EOF). Their evolutions for three El Niño events (1983, 1998, and 2016) are highlighted with lines connecting the dots for the months between January of the first El Niño year and December of the second year. (b) Patterns of $-\nabla \cdot \vec{Q}$ (EP and CP) associated with E and C indices. Indices that are defined as in Ref. [23] from the HadISST data. The dates of $-\nabla \cdot \vec{Q}$ were used from the ERA-Interim reanalysis for the period 1979–2016.

3.2. Observed Rainfall, \vec{Q} , and $-\nabla \cdot \vec{Q}$ during Strong El Niño Events

Figure 5a,b shows patterns of rainfall anomalies and moisture convergence, which indicate how moisture and rainfall configure in the EP and northern Perú-Ecuador during El Niño 1983–1998 and 2016. In the first two events, a notorious zone of \vec{Q} convergence ($-\nabla \cdot \vec{Q}$) that reaches Ecuador and northern Perú (around 4° S) is channeled along the EP and dissipates at the Andes. In the Amazon basin, along 4° S, a dry divergent flow is noted in both El Niños (1983 and 1998). In addition to the

barrier of the Andes that divides the two rainfall regimes (the EP and the Amazon), the subsidence in the Amazon appears as the dominant feature. On the contrary, in the 2016 event, the belt of moist convergence ($-\nabla \cdot \vec{Q}$, a weak case but significant) moves north (around 4° N), confined in the east by the Andes and in the south by northern Perú (around 4° S; Figure 5b and Figure S1). The patterns along the Andes (4° S– 2° N) are similar in the three cases (positive precipitation anomaly) but with a difference in the humidity source in the 2016 case: the \vec{Q} points out of the Andes toward the EP, and a major contribution is from the Amazon. The analysis with \vec{Q} and $-\nabla \cdot \vec{Q}$ suggests that precipitation in this band along the Andes Mountains migrates north–south due to the local effect but is modulated by the moisture transport ($-\nabla \cdot \vec{Q}$) at the large-scale circulation. It was suggested that the warming of SST in the Niño 1 + 2 enhances the diurnal cycle of precipitation forced by the land-sea breeze circulation of the westerly flow that facilitates orographic lifting of moist air and triggers convection [9,11,48]. Interestingly, the 2016 event, unlike El Niño 1983 (and 1998), exhibits an important \vec{Q} flux from the Amazon that reaches the Andes, so the moist air from the ocean is less relevant. This pattern seems to be connected to the convergence in the EP near 4° N, where the convection was migrated. Our analysis suggests that the Amazonian flux provides the necessary moisture to trigger convection in the Andes band. The Amazonian flux comes mainly from lower (900 hPa; the Pacific land-sea breeze) and middle (700 hPa; the Amazonian flux) levels. In 2016, over the south Pacific (near 8° S), \vec{Q} divergence is linked to southerly winds with opposite configuration to the 1983–1998 event (Figure 5b, upper panel). Therefore, the well-known south Pacific semi-permanent anticyclone is not necessarily a positive feedback sign that weakens the El Niño but might be a positive feedback connected via upper circulation. It allows moist air transport in the Amazonia similar to La Niña years, which at the end, could be an important mechanism for triggering convection in the northern region.

The out-of-phase and marked difference between the Pacific and Amazon basin is also observed in vertical levels. In 1998–1983, the Pacific side observes a strong \vec{Q} convergence linked to strong upward motions noted in upper vertical levels of high specific moisture that reaches 500 hPa (Figure 6a). In 2016, a moderate \vec{Q} divergence in the Pacific is linked to downward motions as suppression of convection with notorious drier air in low levels reaching only 800 hPa (Figure 6a). In the Amazon basin, this behavior is opposite but follows the same explanation. These results suggest that the two events (1983–1998 and 2016) have similar drivers as measured by the \vec{Q} convergence: the large-scale atmospheric patterns are from the same source. Although there are differences in the \vec{Q} convergence magnitudes (in both cases 1983–1998 and 2016), responses associated with rainfall variability in the EP responds to the same mechanism. Both 1983–1998 and 2016 have similar large-scale circulation drivers as represented by SST. However, the atmospheric difference on a large-scale is noted with respect to the 2016 event, which is opposite from the 1983–1998 event. The analysis implies that opposed vertical movement of large-scale (i.e., subsidence or ascent motion due to changes in the Walker circulation) forced by SST anomalies [49,50] can lead to convergence patterns of preferential position over the Pacific or Amazonian basin, which represent the out-of-phase pattern that characterizes the moisture source in the EP. This analysis supports the hypothesis that rainfall in the EP can experience opposite out-of-phase patterns in similar El Niño 3.4. In light of these results, in the following step, we take a close look at the mechanism that determines the differences in the meridional extension of \vec{Q} convergence by EP between the two events.

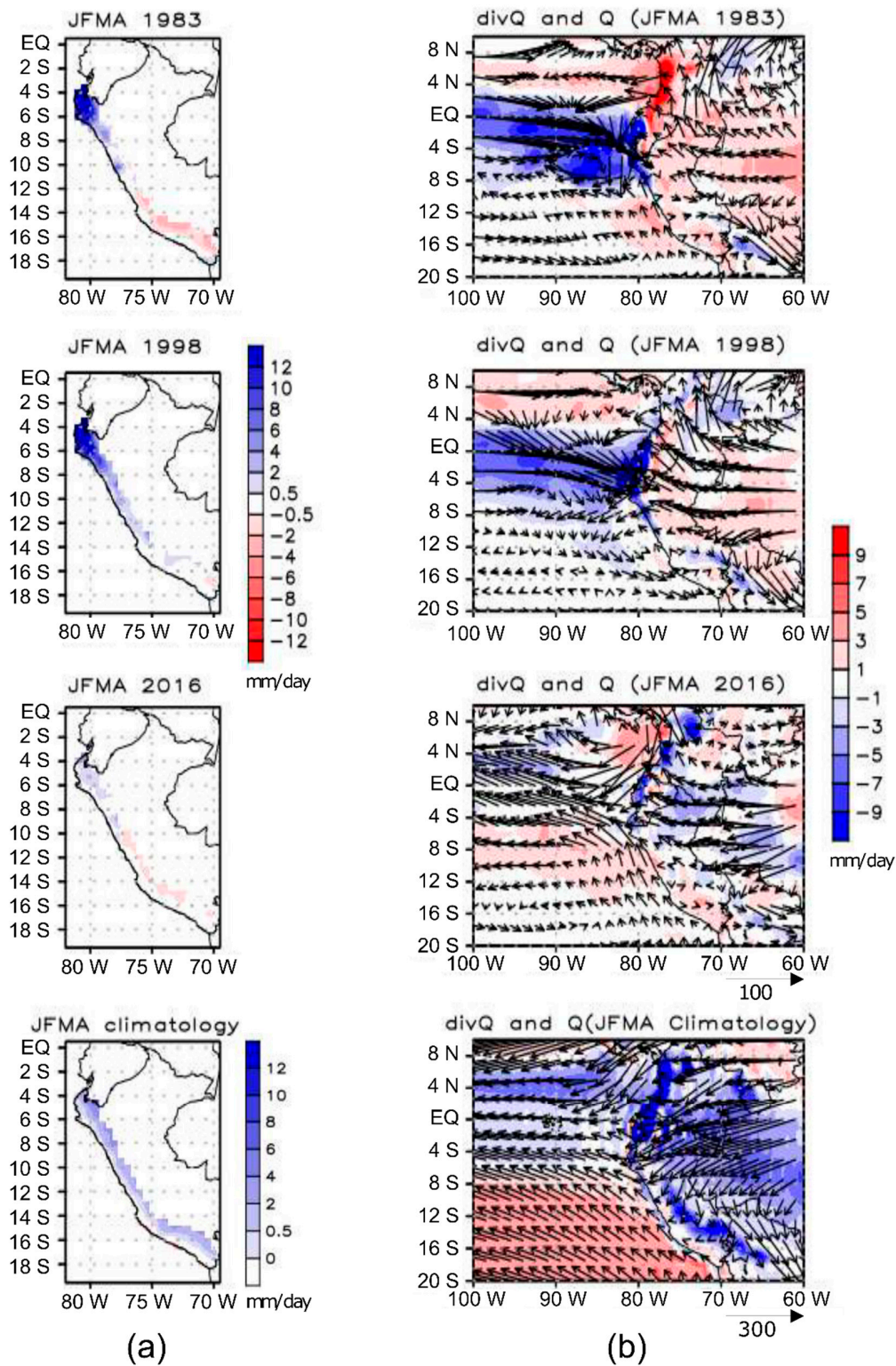


Figure 5. January through April (JFMA) composites of observed precipitation anomalies (mm/day) over the Peruvian coastal region (a), JFMA composites of vertically integrated water vapor transport (\vec{Q}) anomalies (vectors with units of $\text{kg m}^{-1} \text{s}^{-1}$) and its convergence ($-\nabla \cdot \vec{Q}$) anomalies (shaded with units of mm/day) (b). The \vec{Q} and $-\nabla \cdot \vec{Q}$ both integrated between 1000 and 1 hPa. The climatology to construct the anomalies was defined over the period 1979–2016. The continuous shading encompasses positive and negative significant values at the 95% confidence level using the Student’s *t*-test.

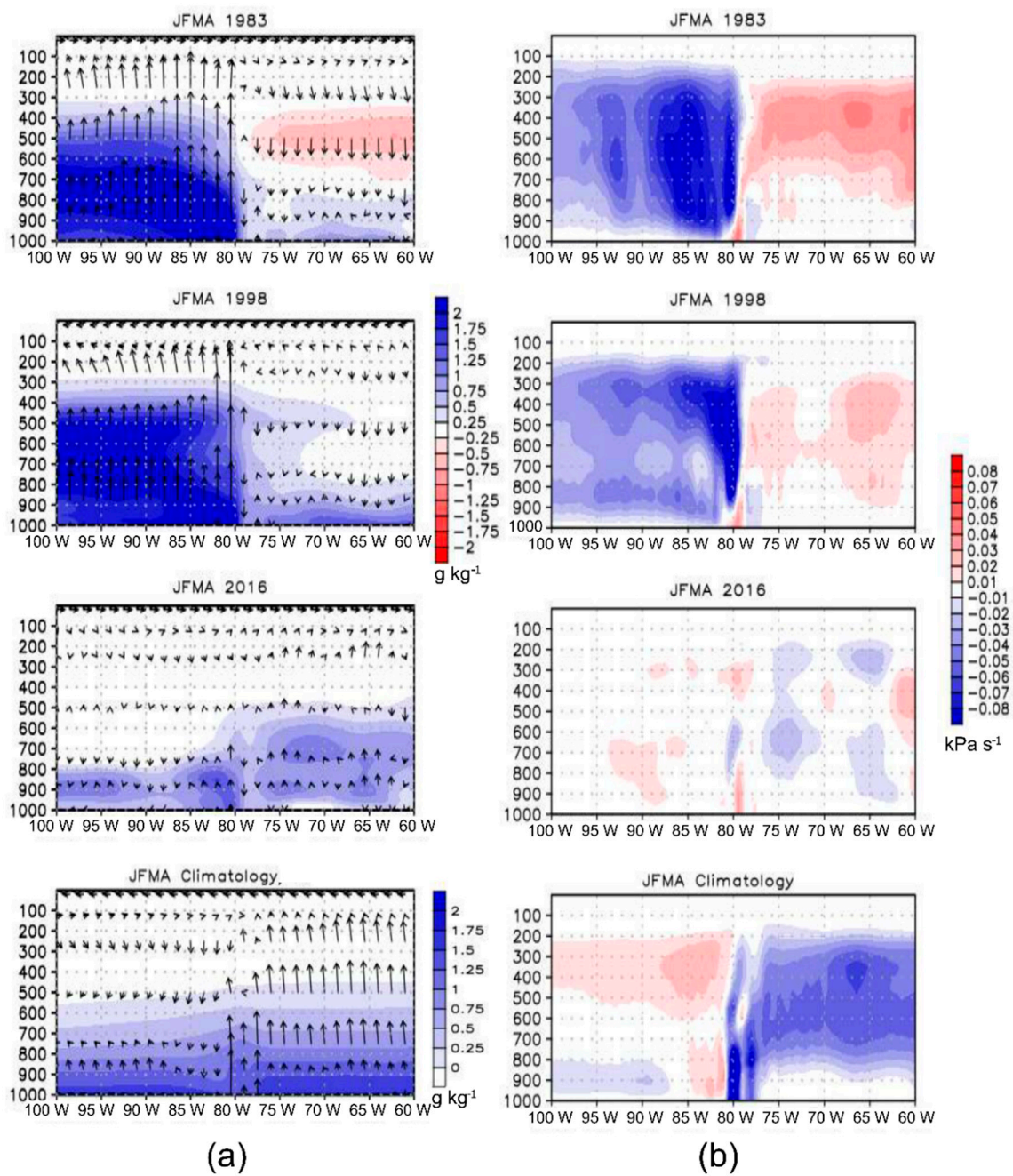


Figure 6. January through April (JFMA) composites of longitude vertical cross-section of specific moisture anomalies (g kg^{-1}) (a) and vertical motion anomalies ω (kPa s^{-1}) (b), for El Niño 1983, 1998, and 2016. The cross-section is averaged over the 2°S and 7.5°S region. Climatology was defined over the 1979–2016 period. The continuous shading indicates significant values at the 95% confidence level using the Student’s *t*-test.

3.3. Global and Regional Driving Mechanisms

Figure 7 depicts the vertical cross-section structure of specific humidity (q) and wind for the three El Niño events, along 2° S through 7.5° S. On the Pacific, during El Niño 2016, a predominant southerly wind is noted in upper levels (200 hPa), which for 1983–1998 is northerly. From previous analysis, it can be inferred that upper-level divergence moves north from its climatological position. The north–south migration is noted in the moisture anomaly of this cross-section with higher values for 1983–1998 than for 2016. Thus, the positive anomaly moisture feeds the deep convection in the EP for 1983–1998. Therefore, the northerly and southerly upper winds modulate the magnitude and extension of rainfall in the EP. Over the Amazon, humidity in mid-levels (700–500 hPa) is a positive anomaly in 2016, which opposes the negative anomaly in 1983. This is consistent with the out-of-phase pattern between El Niño 2016 and 1983. We think the 2016 precipitation response to El Niño is related to the observed global warming in recent years [51–55]. The north migration of upper-level (100 to 300 hPa) winds is linked to moisture influx coming from Amazonian in El Niño 2016 (Figure 7a,b), due to the relaxation of the suppression on the Amazon. In the 1983 event, these high-level divergent winds move south and strengthen the large-scale subsidence over the Amazon, blocking the moisture transport toward the Andes (Figure 7a). The regional mechanism is driven by a continental land-sea breeze with impact in the tropical Andes. In both cases, the Andes is fed by positive anomalies of moist air. The only differences are the sources of the dominant humidity. During 2016, it comes from the Amazon, and from 1983 to 1998, it comes from the Pacific Ocean. The low-level specific humidity (850 hPa; Figure 7) is coherent with the pattern of the \vec{Q} flux band in the EP (Figure 4b) and in El Niño 2016, humidity is concentrated in the coastal region (80° W), and \vec{Q} flux moves away from the coast of northern Perú and Ecuador for this case; therefore, the regional scale of the land-sea breeze is responsible for the deep convection in the tropical Andes.

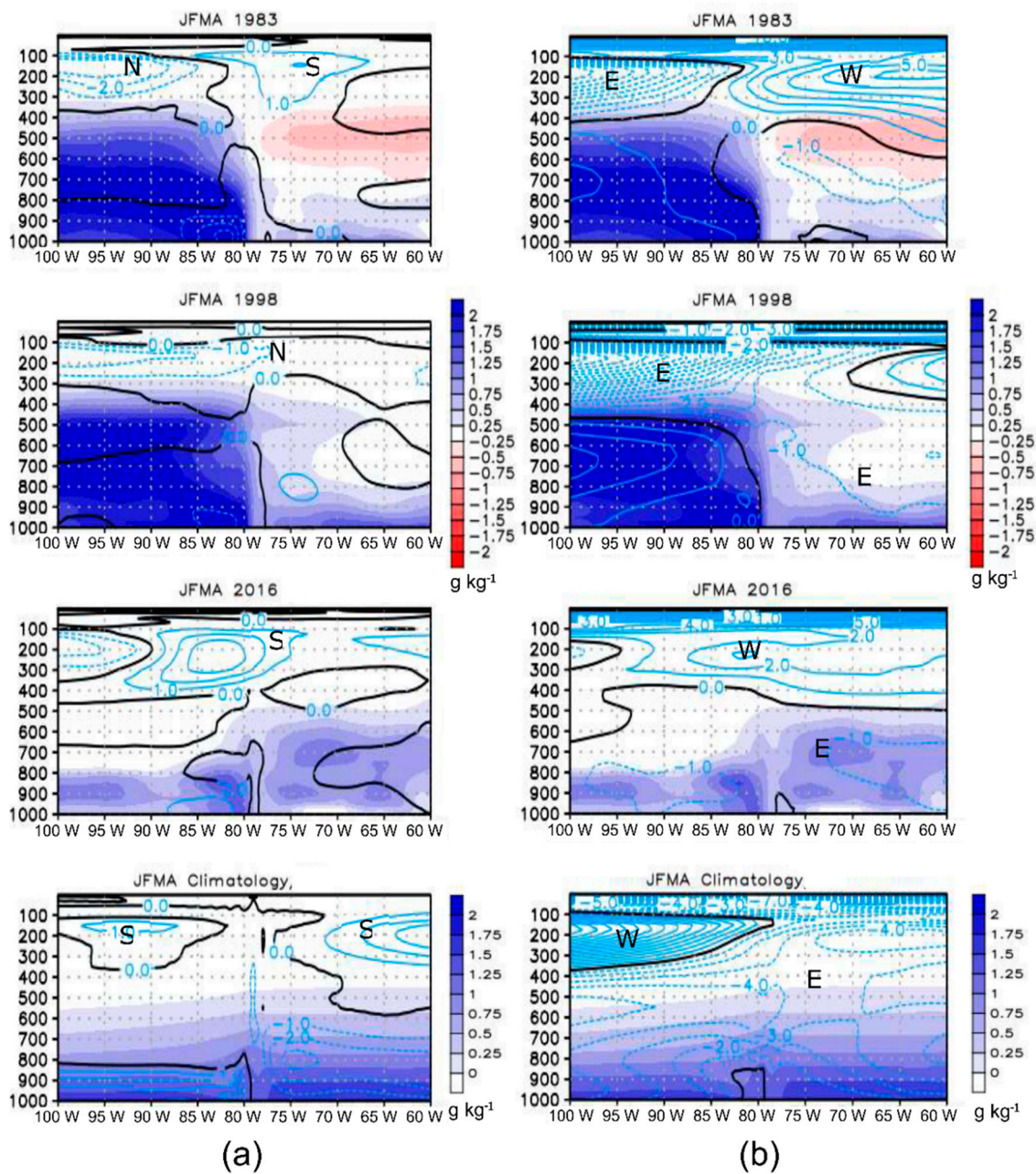


Figure 7. January through April (JFMA) composites of specific moisture vertical cross-section for El Niño 1983, 1998, and 2016. The specific moisture anomalies (g kg^{-1}) in shaded color is superimposed with meridional wind anomalies (m s^{-1}) in colored lines from the south (north) indicated by positive (solid lines) (negative (dotted lines)) values (a) and zonal wind anomalies (m s^{-1}) from the western (eastern) indicated by positive (solid lines) (negative (dotted lines)) values (b). Solid black lines are the zero values that highlight the transition from negative to positive values. The average is computed between 2° S and 7.5° S . Respective climatology is defined over the 1979–2016 period. The continuous shading indicates significant values at the 95% confidence level using the Student’s *t*-test.

4. Conclusions

This study evaluates whether moisture transport from the Amazon could be responsible for extreme rainfall in both the Eastern Pacific (EP) basin and the Andes-in the tropics of Ecuador and northern Perú. Our results suggest that the EP can experience opposite (out-of-phase) patterns of precipitation in “similar” El Niño events; however, the precipitation pattern in the Andes shows no change. We used the reanalysis of the Era-interim-during the last three El Niños 1983, 1998, and 2016 to evaluate regional and large-scale continental spatiotemporal variability concerning the occurrence of extreme rainfall. This analysis assessed atmospheric moisture transport (\vec{Q}) with a focus on water vapor sources and moisture convergence ($-\nabla \cdot \vec{Q}$) as a proxy for precipitation.

Although the strongest El Niño 1983–1998 and 2016, evaluated in the 1950–2016 period, have similar large-scale circulation drivers (Niño 3.4), El Niño 2016 has a clear out-of-phase rainfall pattern at a regional scale in the EP. This precipitation pattern is consistent with the transport of moisture and atmospheric subsidence of vertical motion. Fundamentally, it is the well-known Walker circulation that can explain the large-scale variability (moisture source contributors). During the wet EP, a descending branch of the Walker cell over the Amazon basin is classically portrayed for the event 1983–1998, and during the dry EP, an ascending branch for the event 2016 is observed (Figure 8). The process is thermodynamically maintained by the anomalous moisture in the EP and the Amazon basin. Therefore, the large-scale atmospheric difference between El Niño 2016 and 1983–1998 involves a coherent opposite out-of-phase pattern associated with dominant subsidence in both regions: the East Pacific (in 2016) and the Amazon basin (for 1983–1998), forced by SST anomalies [48,49]. Thus, convection during El Niño 2016 migrated north around 4° N from its climatological Niño position (South around 4° S), which is sustained by moist air from the Amazon basin and a strengthened sub-tropical anticyclone. As El Niño 2016 exhibits $-\nabla \cdot \vec{Q} < 0$ over the Amazon, this flow eventually reaches the highlands of northern Perú and Ecuador.

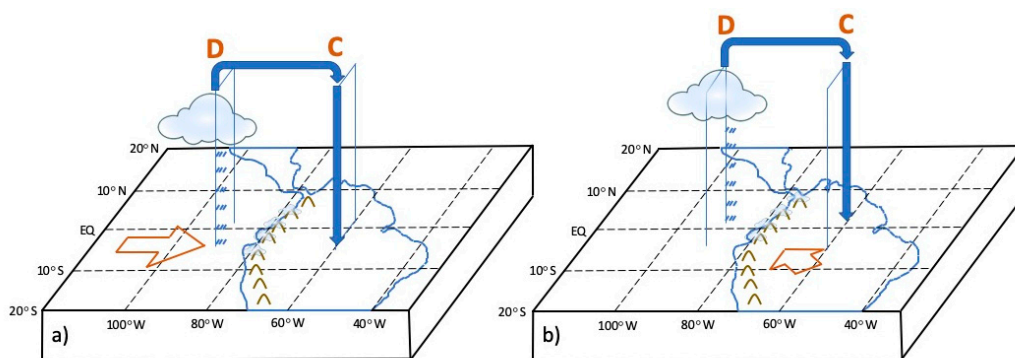


Figure 8. A schematic diagram of the Walker circulation cell during El Niño: 1983–1998 (a) and 2016 (b). The letter D indicates the upper-level divergence, and the letter C the convergence. The big arrows indicate the low-level moist transport.

While the Andes blocked the transport of moisture, $-\nabla \cdot \vec{Q}$, from entering the EP during the 1983–1998 El Niño, $-\nabla \cdot \vec{Q}$ was influenced by regional atmospheric circulation of middle levels (700 hPa) during 2016, which can support and trigger a low-middle level moisture influx coming from the Amazon (Figure 6). The enhanced $-\nabla \cdot \vec{Q}$ is reflected in the different rainfall patterns along the Andes. The anomalous convection in the Amazon facilitates the dry subsidence in the EP to match the water balance associated with this circulation. However, precipitation along the Andes (4° S, 2° N) shows no changes to a dry sign due to a regional land-sea breeze effect noted at low levels (900 hPa) in the Pacific and clearly exceeding the range of the climatology (Figure 7). The extended band of available humidity and land-sea breeze mechanism triggers convection by orographic uplifting [9–11,48,56], but the results presented here are limited to the evaluation of only one case, which is, unfortunately,

the status of the available data. In the EP, the $-\nabla \cdot \vec{Q}$ from the Pacific and Amazonian regions seems to be more important than local processes to suppress rainfall in the 2016 case. Instead, the orographic convection due to the limited—but important—transport moisture seems to be the main mechanism still generating rainfall along the Andes. Therefore, the Andes will experience extreme rainfall over this out-of-phase Niño.

The complexity of El Niño related to rainfall in the EP and the tropical Andes needs to consider other factors, such as the quasi-biennial oscillation (QBO) and the South American low-level jet. An extended analysis could reveal a more comprehensive role of moisture transport in the EP and the Andes regions, which might have implications in its prediction during strong El Niño events. The authors are aware that this work is based on one realization, as this is the first case documented. Therefore, determining statistical thresholds of the role of moisture may help to inform stakeholders about extreme rainfall in order to manage flood risk prevention. In a scenario where enhanced moisture flows from both the Pacific and Amazonia concur, it would intensify convection similar to El Niño 2016 and generate serious impacts with fatalities throughout the region, leading to floods and landslides, causing damages with serious implications in the productive sectors and economic services for these countries [15,57,58].

Supplementary Materials: The following are available online at <http://www.mdpi.com/2073-4433/10/12/768/s1>, Figure S1: January through April (JFMA) composite of (a) the vertically integrated water vapor transport (\vec{Q}) anomalies ($\text{kg m}^{-1} \text{s}^{-1}$; in vectors) and its convergence ($-\nabla \cdot \vec{Q}$) (mm/day; in shaded) for El Niño 1983, 1998 and 2016. The \vec{Q} and $-\nabla \cdot \vec{Q}$ were integrated between 1000 and 300 hPa. The shading also indicates significant values at the 95% level using the Student's *t*-test.

Author Contributions: J.S., C.M.C., and D.L. designed the study, carried out the analysis, and wrote the paper.

Funding: This research was funded by the Peruvian Ministry of Education under the MINEDU-PRONABEC scholarship.

Acknowledgments: The authors would like to thank the Peruvian National Weather (SENAMHI) for providing the observed dataset.

Conflicts of Interest: The authors declare no conflict of interest.

References

1. Bjerknes, J. Atmospheric teleconnections from the equatorial Pacific. *Mon. Weather Rev.* **1969**, *97*, 163–172. [[CrossRef](#)]
2. Rasmusson, E.M.; Carpenter, T.H. Variations in tropical sea surface temperature and surface wind fields associated with the Southern Oscillation/El Niño. *Mon. Weather Rev.* **1982**, *110*, 354–384. [[CrossRef](#)]
3. Deser, C.; Wallace, J.M. El Niño events and their relation to the Southern Oscillation: 1925–1986. *J. Geophys. Res.* **1987**, *92*, 14189–14196. [[CrossRef](#)]
4. Davey, M.K.; Brookshaw, A.; Ineson, S. The probability of the impact of ENSO on precipitation and near-surface temperature. *Clim. Risk Manag.* **2014**, *1*, 5–24. [[CrossRef](#)]
5. McPhaden, M.J.; Zebiak, S.E.; Glantz, M.H. ENSO as an integrating concept in Earth science. *Science* **2006**, *314*, 1740–1745. [[CrossRef](#)] [[PubMed](#)]
6. Ropelewski, C.H.; Halpert, S. Global and regional scale precipitation patterns associated with the El Niño/Southern Oscillation. *Mon. Weather Rev.* **1987**, *115*, 1606–1626. [[CrossRef](#)]
7. Quiroz, R.S. The climate of the “El Niño” winter of 1982–83—A season of extraordinary climatic anomalies. *Mon. Weather Rev.* **1983**, *111*, 1685–1706. [[CrossRef](#)]
8. Barnett, T.P. Interaction of the monsoon and Pacific trade wind system at interannual time scales. Part III: A partial anatomy of the Southern Oscillation. *Mon. Weather Rev.* **1984**, *112*, 2388–2400. [[CrossRef](#)]
9. Horel, J.D.; Cornejo-Garrido, A.G. Convection along the coast of northern Peru during 1983: Spatial and temporal variation of clouds and rainfall. *Mon. Weather Rev.* **1986**, *114*, 2091–2105. [[CrossRef](#)]
10. Goldberg, R.A.; Tisnado, G.M.; Scofield, R.A. Characteristics of extreme rainfall events in northwestern Peru during the 1982–1983 El Niño period. *Geophys. Res. Lett.* **1987**, *92*, 14225–14241. [[CrossRef](#)]

11. Takahashi, K. The atmospheric circulation associated with extreme rainfall events in Piura, Peru, during the 1997–1998 and 2002 El Niño events. *Ann. Geophys.* **2004**, *22*, 3917–3926. [[CrossRef](#)]
12. Bourrel, L.; Rau, P.; Dewitte, B.; Labat, D.; Lavado, W.; Coutaud, A.; Vera, A.; Alvarado, A.; Ordoñez, J. Low-frequency modulation and trend of the relationship between ENSO and precipitation along the northern to centre Peruvian Pacific coast. *Hydrol. Process.* **2016**, *29*, 1252–1266. [[CrossRef](#)]
13. Sanabria, J.; Bourrel, L.; Dewitte, B.; Frappart, F.; Rau, P.; Soils, O.; David, L. Rainfall along the coast of Peru during strong El Niño events. *Int. J. Climatol.* **2018**, *38*. [[CrossRef](#)]
14. Sulca, J.; Takahashi, K.; Espinoza, J.; Vuille, M.; Lavado, W. Impacts of ENSO flavors and tropical Pacific convection variability (ITCZ, SPCZ) on austral summer rainfall in South America focused on Peru. *Int. J. Clim.* **2017**. [[CrossRef](#)]
15. Morata, C.R.; Ballesteros, J.A.; Rohrer, M.; Stoffel, M. The anomalous 2017 coastal El Niño event in Peru. *Clim. Dyn.* **2018**. [[CrossRef](#)]
16. Garreaud, R.D. Short Communication A plausible atmospheric trigger for the 2017 coastal El Niño. *Int. J. Climatol.* **2018**, *38*, e1296–e1302. [[CrossRef](#)]
17. Garreaud, R.D. Intraseasonal variability of moisture and rainfall over the South American Altiplano. *Mon. Weather Rev.* **2000**, *128*, 3337–3346. [[CrossRef](#)]
18. Eichler, T.P.; Londoño, A.C. South American climatology and impacts of El Niño in NCEP’s CFSR data. *Adv. Meteorol.* **2013**, 2013. [[CrossRef](#)]
19. Pineda, L.; Ntegeka, V.; Willems, P. Rainfall variability related to sea surface temperature anomalies in a Pacific-Andean basin into Ecuador and Peru. *Adv. Geosci.* **2013**, *33*, 53–62. [[CrossRef](#)]
20. Gimeno, L.; Dominguez, F.; Nieto, R.; Trigo, R.; Drumond, A.; Reason, C.J.C.; Kumar, R.; Marengo, J. Major Mechanisms of Atmospheric Moisture Transport and their Role in Extreme Precipitation Events. *Annu. Rev. Environ. Resour.* **2016**, *41*, 117–141. [[CrossRef](#)]
21. Garreaud, R.D. The Andes climate and weather. *Adv. Geosci.* **2009**, *7*, 1–9. [[CrossRef](#)]
22. Kao, H.Y.; Yu, J.Y. Contrasting Eastern-Pacific and Central-Pacific types of ENSO. *J. Clim.* **2009**, *22*, 615–632. [[CrossRef](#)]
23. Takahashi, K.; Montecinos, A.; Goubanova, K.; Dewitte, B. ENSO regimes: Reinterpreting the canonical and Modoki El Nio. *Geophys. Res. Lett.* **2011**. [[CrossRef](#)]
24. Capotondi, A.; Wittenberg, A.T.; Newman, M.; Di Lorenzo, E.; Yu, J.-Y.; Braconnot, P.; Cole, J.; Dewitte, B.; Giese, B.; Guilyardi, E.; et al. Understanding ENSO diversity. *Bull. Am. Meteorol. Soc.* **2015**, *96*, 921–938. [[CrossRef](#)]
25. Vecchi, G.A. The termination of the 1997–98 El Niño. Part II: Mechanisms of atmospheric change. *J. Clim.* **2006**, *19*, 2647–2664. [[CrossRef](#)]
26. Takahashi, K.; Battisti, D.S. Processes controlling the mean tropical Pacific precipitation pattern. Part II: The SPCZ and the Southeast Pacific dry zone. *J. Clim.* **2007**, *20*, 5696–5706. [[CrossRef](#)]
27. Tedeschi, R.G.; Cavalcanti, I.F.A.; Grimm, A.M. Influences of two types of ENSO on South American precipitation. *Int. J. Climatol.* **2013**, *33*, 1382–1400. [[CrossRef](#)]
28. Waliser, D.E.; Gautier, C. A satellite-derived climatology of the ITCZ. *J. Clim.* **1993**, *6*, 2162–2174. [[CrossRef](#)]
29. L’Heureux, M.L.; Takahashi, K.; Watkins, A.B.; Barnston, A.G.; Becker, E.J.; Di Liberto, T.E.; Gamble, F.; Gottschalck, J.; Halpert, M.S.; Huang, B.; et al. Observing and Predicting the 2015–16 El Niño. *Bull. Amer. Meteorol. Soc.* **2016**. [[CrossRef](#)]
30. Levine, A.F.Z.; McPhaden, M.J. How the July 2014 easterly wind burst gave the 2015–2016 El Niño a head start. *Geophys. Res. Lett.* **2016**, *43*, 6503–6651. [[CrossRef](#)]
31. Paek, H.Y.; Qian, J.-Y.C. Why were the 2015/16 and 1997/98 Extreme El Niños different? *Geophys. Res. Lett.* **2017**, *44*, 1848–1856. [[CrossRef](#)]
32. Hu, S.; Fedorov, A.V. The extreme El Niño of 2015–2016: The role of westerly and easterly wind bursts, and preconditioning by the failed 2014 event. *Clim. Dyn.* **2017**, 1–19. [[CrossRef](#)]
33. Paixao Veiga, J.A.; Rao, V.B.; Franchito, S.H. Heat and moisture budgets of the walker circulation and associated rainfall anomalies during El Niño events. *Int. J. Climatol.* **2005**, *25*, 193–213. [[CrossRef](#)]
34. Rau, P.; Bourrel, L.; Labat, D.; Melo, P.; Dewitte, B.; Frappart, F.; Lavado, W.; Felipe, O. Regionalization of rainfall over the Peruvian Pacific slope and coast. *Int. J. Climatol.* **2017**, *37*, 143–158. [[CrossRef](#)]

35. Simmons, A.; Uppala, S.; Dee, D.; Kobayashi, S. ERA-Interim: New ECMWF Reanalysis Products from 1989 Onwards. *ECMWF Newsl.* **2006**, *110*, 25–35. Available online: www.ecmwf.int/publications/newsletters (accessed on 3 November 2019).
36. Dee, D.P.; Uppala, S.M.; Simmons, A.J.; Berrisford, P.; Poli, P.; Kobayashi, S.; Andrae, U.; Balmaseda, M.A.; Balsamo, G.; Bauer, P.; et al. The ERA-Interim reanalysis: Configuration and performance of the data assimilation system. *Q.J. R. Meteorol. Soc.* **2011**, *137*, 553–597. [[CrossRef](#)]
37. Lorenz, C.; Kunstmann, H. The hydrological cycle in three state-of-the-art reanalyses: Intercomparison and performance analysis. *J. Hydrometeorol.* **2012**, *13*, 1397–1420. [[CrossRef](#)]
38. Solman, S.A.; Sanchez, E.; Samuelsson, P.; da Rocha, R.P.; Li, L.; Marengo, J.; Pessacq, N.L.; Remedio, A.R.C.; Chou, S.C.; Berbery, H.; et al. Evaluation of an ensemble of regional climate model simulations over South America driven by the ERA-Interim reanalysis: Model performance and uncertainties. *Clim. Dyn.* **2013**, *41*, 1139–1157. [[CrossRef](#)]
39. Knippertz, P.; Wernli, H.; Gläser, G. A global climatology of tropical moisture exports. *J. Clim.* **2013**, *26*, 3031–3045. [[CrossRef](#)]
40. Drumond, A.; Marengo, J.; Ambrizzi, T.; Nieto, R.; Moreira, L.; Gimeno, L. The role of the Amazon Basin moisture in the atmospheric branch of the hydrological cycle: A Lagrangian analysis. *Hydrol. Earth Syst. Sci.* **2014**, *18*, 2577–2598. [[CrossRef](#)]
41. Trenberth, K.E.; Fasullo, J.T.; Mackaro, J. Atmospheric moisture transports from ocean to land and global energy flows in reanalyses. *J. Clim.* **2011**, *24*, 4907–4924. [[CrossRef](#)]
42. Sohn, B.-J.; Smith, E.A.; Robertson, F.R.; Park, S.-C. Derived over-ocean water vapor transports from satellite-retrieved E–P data-sets. *J. Clim.* **2004**, *17*, 1352–1365. [[CrossRef](#)]
43. Mo, R.; Straus, D. Statistical–Dynamical Seasonal Prediction Based on Principal Component Regression of GCM Ensemble Integrations. *Mon. Weather Rev.* **2002**, *130*, 2167–2187. [[CrossRef](#)]
44. Peixoto, J.P.; Oort, A.H. Physics of Climate. In *American Institute of Physics*; MIT press: San Diego, CA, USA, 1992; p. 520.
45. Dacre, H.F.; Clark, P.A.; Martinez-Alvarado, O.; Stringer, M.A.; Lavers, D.A. How do atmospheric rivers form? *Bull. Am. Meteorol. Soc.* **2015**, *96*, 1243–1255. [[CrossRef](#)]
46. Allan, R.P.; Lavers, D.A.; Champion, A.J. Diagnosing links between atmospheric moisture and extreme daily precipitation over the UK. *Int. J. Climatol.* **2016**, *36*, 3191–3206. [[CrossRef](#)]
47. Ramage, C.S.; Hori, A.M. Meteorological aspects of El Niño. *Mon. Weather Rev.* **1981**, *109*, 1827–1835. [[CrossRef](#)]
48. Douglas, M.W.; Mejia, J.; Ordinola, N.; Boustead, J. Synoptic Variability of Rainfall and Cloudiness along the Coasts of Northern Peru and Ecuador during the 1997/98 El Niño Event. *Mon. Weather Rev.* **2009**, *137*, 116–136. [[CrossRef](#)]
49. Ambrizzi, T.E.; De Souza, B.; Pulwarty, S.R. The Hadley and Walker regional circulations and associated ENSO impacts on South American seasonal rainfall. In *Hadley Circulation: Present, Past and Future; Advances in Global Change Research*; Diaz, H.F., Bradley, R.S., Eds.; Springer: Dordrecht, The Netherlands, 2004; Volume 21, pp. 203–235. [[CrossRef](#)]
50. Shimizu, M.H.; Ambrizzi, T.; Liebmann, B. Extreme precipitation events and their relationship with ENSO and MJO phases over northern South America. *Int. J. Climatol.* **2016**. [[CrossRef](#)]
51. Hu, S.; Fedorov, A.V. The extreme El Niño of 2015–2016 and the end of global warming hiatus. *Geophys. Res. Lett.* **2017**, *44*. [[CrossRef](#)]
52. Power, S.; Delage, F.; Chung, C.; Kociuba, G.; Keay, K. Robust twenty-first-century projections of El Niño and related precipitation variability. *Nature* **2013**, *502*, 541–545. [[CrossRef](#)]
53. Santoso, A.; McGregor, S.; Jin, F.F.; Cai, W.; England, M.H.; An, S.I.; McPhaden, M.J.; Guilyardi, E. Late-twentieth-century emergence of the El Niño propagation asymmetry and future projections. *Nature* **2013**, *504*, 126–130. [[CrossRef](#)] [[PubMed](#)]
54. Cai, W.; Borlace, S.; Lengaigne, M.; van Rensch, P.; Collins, M.; Vecchi, G.; Timmermann, A.; Santoso, A.; McPhaden, M.J.; Wu, L.; et al. Increasing frequency of extreme El Niño events due to greenhouse warming. *Nat. Clim. Chang.* **2014**, *4*, 111–116. [[CrossRef](#)]
55. Medhaug, I.; Stolpe, M.B.; Fischer, E.M.; Knutti, R. Reconciling controversies about the global warming hiatus'. *Nature* **2017**, *545*, 41–47. [[CrossRef](#)] [[PubMed](#)]

56. Bendix, J. Precipitation dynamics in Ecuador and northern Peru during the 1991/92 El Niño: A remote sensing perspective. *Int. J. Remote Sens.* **2000**, *21*, 533–548. [[CrossRef](#)]
57. Di Liberto, T. Heavy Summer Rains Flood Peru. NOAA, 2017. Available online: <https://www.climate.gov/news-features/event-tracker/heavy-summer-rains-flood-peru> (accessed on 3 November 2019).
58. Ramirez, I.; Briones, F. Understanding the El Niño Costero of 2017: The Definition Problem and Challenges of Climate Forecasting and Disaster Responses. *Int. J. Disaster Risk Sci.* **2017**, *8*, 489–492. [[CrossRef](#)]



© 2019 by the authors. Licensee MDPI, Basel, Switzerland. This article is an open access article distributed under the terms and conditions of the Creative Commons Attribution (CC BY) license (<http://creativecommons.org/licenses/by/4.0/>).